

# 1 Ultrasonic Implantation and Imaging of Sound-Sensitive 2 Theranostic Agents for the Treatment of Arterial Inflammation

3 Xiaoqian Su,<sup>#</sup> Moumita Rakshit,<sup>#</sup> Prativa Das, Ipshita Gupta, Dhiman Das, Manojit Pramanik,<sup>\*</sup>  
4 Kee Woei Ng,<sup>\*</sup> and James Kwan<sup>\*</sup>



Cite This: <https://doi.org/10.1021/acsami.1c01161>



Read Online

ACCESS |



Metrics & More



Article Recommendations

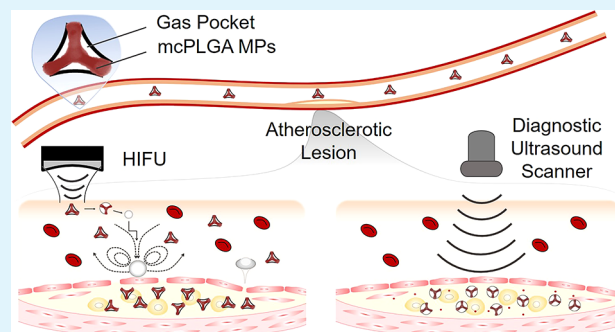


Supporting Information

5 **ABSTRACT:** For site-specific diseases such as atherosclerosis, it is  
6 desirable to noninvasively and locally deliver therapeutics for  
7 extended periods of time. High-intensity focused ultrasound  
8 (HIFU) provides targeted drug delivery, yet remains unable to  
9 sustain delivery beyond the HIFU treatment time. Furthermore,  
10 methods to validate HIFU-enhanced drug delivery remain limited. In  
11 this study, we report on HIFU-targeted implantation of degradable  
12 drug-loaded sound-sensitive multicavity PLGA microparticles  
13 (mcPLGA MPs) as a theranostic agent for the treatment of arterial  
14 lesions. Once implanted into the targeted tissue, mcPLGA MPs  
15 eluted dexamethasone for several days, thereby reducing inflamma-  
16 tory markers linked to oxidized lipid uptake in a foam cell spheroid

17 model. Furthermore, implanted mcPLGA MPs created hyperechoic regions on diagnostic ultrasound images, and thus noninvasively  
18 verified that the target region was treated with the theranostic agents. This novel and innovative multifunctional theranostic platform  
19 may serve as a promising candidate for noninvasive imaging and treatment for site-specific diseases such as atherosclerosis.

20 **KEYWORDS:** Therapeutic Ultrasound, Ultrasound Contrast Enhancement, Atherosclerosis, Anti-Inflammatories, Dexamethasone



## 1. INTRODUCTION

21 Cardiovascular diseases (CVD) account for the highest  
22 mortality rates worldwide, and incidences have been  
23 dramatically increasing due to lifestyle-related factors and  
24 aging populations.<sup>1</sup> Among CVDs, atherosclerosis accounts for  
25 a majority of the reported morbidity and mortality.<sup>2</sup>  
26 Atherosclerosis is an inflammatory disease caused by hardening  
27 of the arterial walls and narrowing of the arteries resulting from  
28 the accumulation of lipids and fibrous tissues within the arterial  
29 intima.<sup>3</sup> These plaques are formed from the buildup of foam  
30 cells that develop from monocytes attracted to the  
31 subendothelial part of the arteries that are rich in lipids. The  
32 monocytes then differentiate into macrophages and excessively  
33 take up and metabolize modified lipoproteins, and in turn  
34 further differentiate into foam cells.<sup>4</sup> These foam cells  
35 accumulate over time and combine into a plaque that slowly  
36 becomes at risk for ruptures that occlude blood vessels and  
37 cause serious health implications.<sup>4–6</sup> Inflammation plays a  
38 major part in the progression of atherosclerosis, and thus anti-  
39 inflammatory drugs are under intense investigation as a  
40 therapeutic.

41 Dexamethasone (Dex) is one of the most used glucocorti-  
42 coids for the treatment of atherosclerosis. Depending on the  
43 concentration, Dex may mitigate inflammation in two  
44 ways—(i) by forming a complex with glucocorticoid receptors  
45 (GR) and binding to nuclear factor kappa B (NFκB), blocking

the downstream transcriptional activation of inflammatory 46  
genes, and (ii) by specific inhibition of proteins that stabilize 47  
mRNA of pro-inflammatory genes leading to lower expression 48  
of these genes.<sup>7,8</sup> In addition to its anti-inflammatory 49  
properties, Dex has shown to be beneficial against cholesterol 50  
accumulation in mice by inhibiting foam cell formation<sup>9</sup> and  
reducing cholesteryl ester accumulation in *in vitro* and *in vivo* 52  
atherogenic mice aorta models.<sup>10–12</sup> 53

At present, Dex is administered orally or intravenously. 54  
However, these delivery methods have limited efficiency 55  
because of the short circulation half-life and nonspecificity of 56  
Dex. As a result, these limitations necessitate repeated 57  
administration, risking systemic exposure to potentially toxic 58  
drug concentrations and reduced patient compliance. Due to 59  
the reliance on drug diffusion from circulation, drugs may not 60  
reside within the diseased tissues at therapeutically effective 61  
levels. Considering these issues and the chronic nature of 62  
atherosclerosis, there has been a shift toward targeted drug 63  
delivery with sustained delivery systems, thereby maximizing 64

Received: January 18, 2021

Accepted: May 10, 2021

therapeutic impacts while keeping side effects to a minimum.<sup>13,14</sup>

Drug-loaded vesicles have potential in achieving sustained and localized drug delivery. Such vesicles include liposomes, polymer micro/nanospheres, and ultrasound-sensitive micro/nanostructures. The small size, large surface area to volume ratio, and mobility in tissue of drug-loaded vesicles make them an ideal choice for targeted therapy by aiding in (i) the penetration across blood-tissue barriers, (ii) circulation, and (iii) internalization.<sup>15</sup> Yet, current drug delivery methods are limited due to the low efficiency in targeting, image-guided positioning accuracy, and distribution of therapeutics throughout the lesion sites. There remains a need for targeted drug delivery of drug-eluting devices that sustain the delivery for a prolonged duration of time after administration to treat chronic diseases.

High-intensity focused ultrasound (HIFU) is a minimally invasive therapeutic technique used for tumor ablation,<sup>16</sup> drug and gene delivery,<sup>17</sup> and blood-brain barrier (BBB) opening.<sup>18</sup> Ultrasound-mediated drug delivery is often driven by acoustic cavitation, i.e., the dynamic oscillations of gas or vapor bubbles, to improve drug distribution<sup>19</sup> and localized release.<sup>20,21</sup> Yet, nucleate cavitation requires substantial acoustic energy capable of damaging off-target healthy tissue. Therefore, preformed cavitation nuclei such as small gaseous particles (microbubbles) are widely used to enable cavitation at reduced acoustic pressure amplitudes.<sup>22,23</sup> As such, microbubbles have been shown to nucleate cavitation and improve the local delivery of therapeutic agents across cancers, cardiovascular diseases, and neurological disorders.<sup>24,25</sup> Despite the many benefits microbubbles provide, microbubbles have disease specific limitations owing to their large size and rapid destruction<sup>26</sup> in an acoustic field. Furthermore, these particles do not extravasate beyond the blood vessel network. Thus, solid cavitation nuclei such as mesoporous silica,<sup>27</sup> polymeric nanocups,<sup>28</sup> and gold nanocones<sup>29</sup> have been put forward with advantages of prolonging cavitation activity, penetrating beyond blood vessels, and be embedded into tissue. Similarly, nonbiodegradable solid cavitation nuclei were shown to sustain cavitation across minutes and improved the distribution of a coadministered drug.<sup>28</sup>

Many imaging modalities, such as ultrasound imaging, X-ray computed tomography (CT), and magnetic resonance imaging (MRI), are used for guiding or validating HIFU-based therapies. Among these imaging modalities, ultrasound imaging has several advantages such as real-time monitoring, high penetration depth, and low cost. By coupling HIFU and diagnostic ultrasound with a sound-sensitive microparticle enable a theranostic approach to administer therapy with real-time guidance and treatment validation. Conventional ultrasound imaging use microbubbles to improve acoustic scattering to create hyperechoic regions in the ultrasound image. The contrast enhancement stems from the gas within these microbubbles, which are highly compressible and are thus more echogenic than the surrounding tissues, thereby enhancing the backscattered ultrasound signal by  $\sim 10$ – $30$  dB.<sup>30</sup> However, this enhancement in contrast typically is limited to the blood vessels and capillaries carrying these microbubbles.

It is therefore desirable to combine the ultrasound contrast enhancement of microbubbles with prolonged cavitation and extravasation potential of solid cavitation nuclei to address the specific needs for treating and imaging chronic site-specific

diseases such as atherosclerosis. Recently, mcPLGA MPs-based HIFU cavitation agents have been developed by our group,<sup>31</sup> which demonstrated the site-specific implantation of drug-loading particles into porcine arterial tissue by HIFU. However, drug loading into these particles was not performed; the therapeutic effect and potential for ultrasound contrast-enhanced imaging from these particles post-implantation have therefore not yet been investigated, and this is the focus of this report. Here, we substantially advance on our previous work to re-engineer an all-in-one degradable ultrasound theranostic agent composed of Dex-loaded mcPLGA MPs (Dex/mcPLGA MPs) with surface-stabilized gas nanobubbles. These mcPLGA MPs are capable of being implanted into tissue in response to HIFU and enhance the echogenicity of the tissue after implantation in response to diagnostic ultrasound. Once implanted, the microparticles hydrolytically degraded to sustain the release of a therapeutic agent at the site of the diseased tissue. We also employed an *in vitro* 3D foam cell spheroid model, to study the anti-atherogenic potential of Dex/mcPLGA MPs. Our study indicated reduced secretion of pro-inflammatory cytokines by the spheroids in response to HIFU+Dex/mcPLGA MPs, which further emphasized the therapeutic benefits of the ultrasound sensitive drug carriers.

## 2. EXPERIMENTAL SECTION

**Materials.** Resomer RG504 H (lactide:glycolide 50:50, Mw 38,000–54,000), Poly(vinyl alcohol) (PVA) (80% hydrolyzed, Mw 9,000–10,000), phosphate buffered saline (PBS) tablet, Dexamethasone (BioReagent,  $\geq 97\%$ ), Rhodamine B (RhB), Dichloromethane (anhydrous,  $\geq 99.8\%$ ), Fluoroshield with DAPI, and Phorbol 12-myristate 13-acetate (PMA) were purchased from Merck. Agarose was purchased from Vivantis Technologies. Human oxidized low density lipoprotein (oxLDL) was obtained from Alfa Aesar by Thermo Fisher Scientific. Fetal bovine serum (FBS) was from Hyclone (Logan, UT, USA). Aggregate culture of foam cells was seeded into Perfecta3D 96-well hanging drop plate (3D Biomatrix, USA).

**Fabrication of mcPLGA MPs.** mcPLGA MPs were prepared using a double emulsion method described in our previous work.<sup>32</sup> In brief, 2 mL of PLGA in DCM (25 mg/mL) was mixed with 0.1 mL of 20 $\times$  PBS and sonicated over ice at 100 W for 30 s to form the primary W/O emulsion. To form the W/O/W emulsion, 10 mL of 5 wt % PVA was added to the primary emulsion and homogenized at 12,000 rpm for 5 min. The obtained W/O/W emulsion was stirred for 2 h in an open container to allow for evaporation of the organic solvent and pores formation. For RhB/Dex loaded mcPLGA MPs, the payload was added into the organic phase before sonication and homogenization following the method described above.

**Characterization of mcPLGA MPs.** FE-SEM and TEM were used to assess the size and morphology of mcPLGA MPs. Samples for SEM and TEM analysis were prepared as described previously.<sup>32</sup> Size distributions were performed on a Malvern Instruments Zetasizer Nano-ZS instrument.

**Encapsulation Efficiency and Release Profile.** The quantity of Dex present and release profile as a function of time was measured by UV-absorbance in solution.<sup>32</sup> The encapsulation efficiency was calculated by the actual amount of drug entrapped (total drug added – free non-entrapped drug) divided by the total amount of drug added initially during preparation. The release profile was determined by the amount of drug delivered (Mt) to the amounts of effectively encapsulated drug ( $M_0$ ), as a function of time.<sup>33</sup>

**HIFU Setup.** Cavitation potential from mcPLGA particles was measured using a conventional HIFU setup (1.1 MHz, 20 cycles, 10 Hz pulse repetition frequency, or PRF).<sup>31</sup> Afterward, the acoustic emissions were collected and post-processed using power FFT to get power spectral density curves. Following that, the cavitation threshold was defined as a 6 dB difference between the received signal from mcPLGA MPs and reference water.

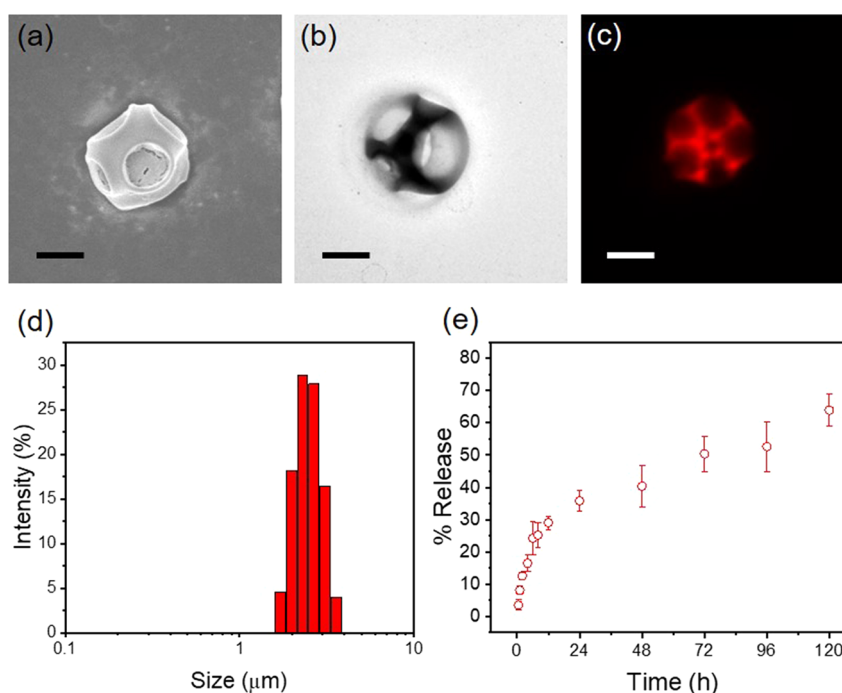


**Figure 1.** Representative SEM (a), TEM (b), and fluorescence (c) image of Dex-loaded mcPLGA MPs (Dex/mcPLGA MPs). Rhodamine B (RhB) was also coloaded to track the location of particles (c). (d) Size of mcPLGA MPs as measured by dynamic light scattering (DLS). (e) Dex release profile *in vitro*. Scale bars represent 1  $\mu\text{m}$ . Three independent experimental sets were performed.

**Diagnostic Ultrasound Setup.** Clinical ultrasound imaging was acquired using a clinical ultrasound system (E-Cube 12-R, Alpinion Medical Systems, South Korea).<sup>34</sup> Scanning was performed with B mode operating at 10 MHz with a mechanical index (MI) of 1.0. Afterward contrast to tissue ratio (CTR) analysis was performed by normalizing the mean squared acoustic power of the backscattered signal from the mcPLGA MPs to the signal of tissue.

**Cell Culture and Spheroid Formation.** THP-1 cells, a human monocytic cell line (ATCC, Rockville, MD), were cultured in Roswell Park Memorial Institute (RPMI) 1640 Medium (Pan Biotech, Germany) supplemented with 100 IU/mL of penicillin, 100  $\mu\text{g}/\text{mL}$  streptomycin (Pan Biotech, Germany), 2 mmol/L L-glutamine, 10% (v/v) FBS (Gibco, USA), and incubated in a humidified atmosphere of 5%  $\text{CO}_2$  in an incubator at 37  $^{\circ}\text{C}$ . The medium was replaced every 2–3 days by centrifuging these suspended cells at 125 g for 5 min. For differentiation of THP-1 monocytes into macrophages, THP-1 cells were seeded at a density of  $7 \times 10^5$  cells/mL with differentiation medium, growth medium supplemented with 50 ng/mL PMA, for 3 days to obtain macrophages. Subsequently, for foam cell induction, macrophages were incubated with 100  $\mu\text{g}/\text{mL}$  oxLDL in the differentiation medium for 2 days.

A three-dimensional (3D) foam cell spheroid model was developed by modification of the hanging drop method.<sup>35</sup> Foam cells were seeded into Perfecta3D 96-well hanging drop plate (3D Biomatrix, USA) at a density of  $1.25 \times 10^6$  cells/mL and incubated for 4 days at 37  $^{\circ}\text{C}$  with 5%  $\text{CO}_2$ . The foam cell spheroids formed were collected and subjected to treatment immediately.

**HIFU Implantation of mcPLGA MPs into Spheroid Studies and Ultrasound Imaging.** To create a spheroid embedded sample chamber for HIFU exposure, spheroids were first embedded into alginate beads. Then, the beads were washed and mounted along the channel of agarose chamber mentioned above. Then, RhB/DAPI-mcPLGA MPs were suspended in PBS (1 mg/mL) and pumped through the channel (0.2 mL/min) for ultrasound exposure (1.1 MHz, 3.2 MPa, 5% duty cycle). After exposure to ultrasound for 5 min, the sample chamber was washed with PBS to remove the remaining mcPLGA MPs and imaged using the therapeutic ultrasound setup described above or collected for further analysis.

The distribution of mcPLGA MPs throughout the spheroids and the release of therapeutics were analyzed using confocal microscope (Zeiss LSM 800). To determine the histological and physiological effects of HIFU mediated delivery of Dex loaded mcPLGA MPs to foam cell spheroids, the spheroids were sectioned (10  $\mu\text{m}$ ) using a Leica CM1950 Cryostat, mounted on glass slides, and stained with Oil Red O to visualize lipid under inverted microscopy (AxioVert 200, Carl Zeiss).

**Cytokine Array.** In order to examine the inflammatory cytokines secreted by foam cell spheroids, cell culture supernatants were collected and subjected to a cytokine array (Human Cytokine Antibody Array (Membrane, 42 Targets); Abcam, USA) according to the manufacturer's instructions. Signal intensities were quantified using the Image Quant software and normalized to the untreated samples.

**Statistical Analysis.** Data presented were representative of 3 independent experiments, and quantitative results were expressed as mean  $\pm$  standard deviation (SD) unless otherwise specified. Data were analyzed by One-Way and Two-Way ANOVA with post hoc Tukey's analysis using Origin Pro 2015 (OriginLab, USA) or Student's *t* test. A *p* value below 0.05 was considered statistically significant.

### 3. RESULTS AND DISCUSSION

The mcPLGA MPs were fabricated following a modified double emulsion method that used PBS as a porogen.<sup>32</sup> The obtained mcPLGA MPs exhibited a mean size of  $2.5 \pm 0.5$   $\mu\text{m}$  with a multitude of surface cavities (Figure 1a–c). The rough cavity inner surface facilitates gas trapping required for ultrasound imaging and ultrasound enhanced drug delivery. Gas trapping into the cavities was accomplished by a drying and resuspension process.<sup>28</sup> No agglomerations were observed as indicated by the polydispersity index (PDI),  $\text{PDI} = 0.13$ , in either deionized water or PBS (Figure 1d).

During fabrication, Dex resided in the oil phases of the emulsion alongside the PLGA polymer. As the oil phase was removed, Dex was trapped in the PLGA matrix with an



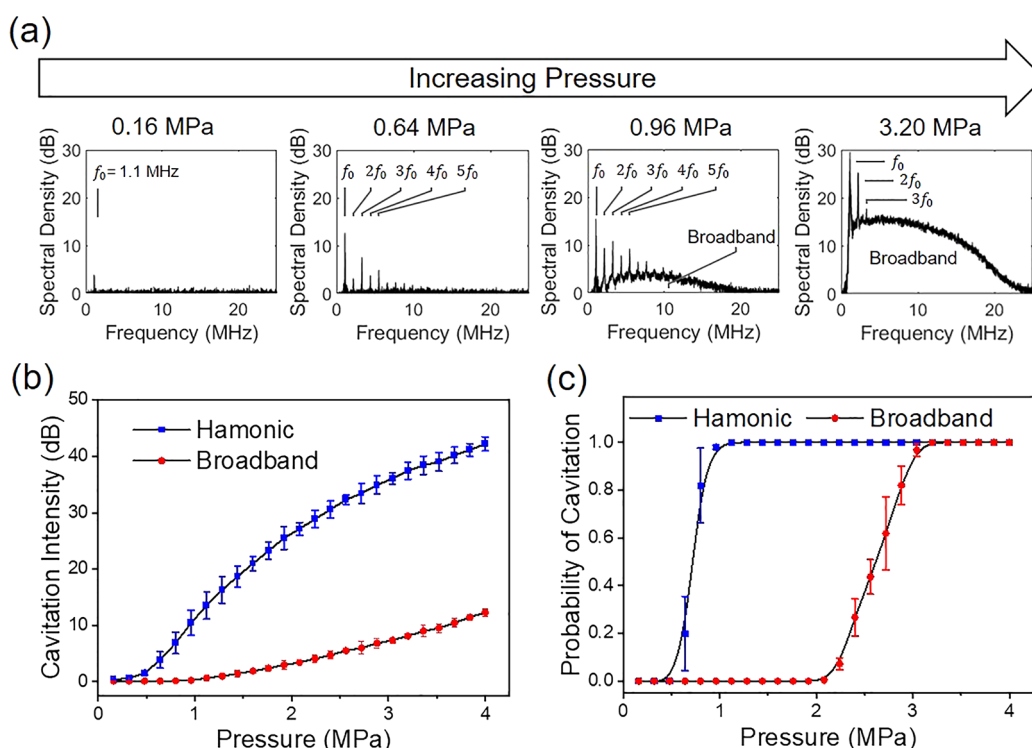


**Figure 2.** Acoustic response of mcPLGA MPs exposed to 1.1 MHz HIFU. (a) Representative spectral density curves of mcPLGA MPs under different exposure pressures. (b) Cavitation intensity and (c) probability of cavitation of mcPLGA MPs.

encapsulation efficiency of  $70.3 \pm 6.9\%$ . Figure 1e shows the release of Dex from mcPLGA MPs in PBS across 5 days. Initially,  $29.1 \pm 5.1\%$  of Dex was released within 12 h. However, it required 5 days to release  $63.9 \pm 7.8\%$  of Dex from mcPLGA MPs, which was consistent with previous observations.<sup>32</sup>

The acoustic responses from mcPLGA MPs were measured using a 1.1 MHz HIFU transducer.<sup>28,31</sup> During exposure to HIFU across a range of pressure amplitudes (0.16–4.0 MPa), we detected both harmonic and broadband signals (Figures 2a and S1). Backscattered signal centered around the fundamental and harmonic frequencies is often attributed to the nonlinear dynamics of cavitation bubbles, indicating the inception of stable cavitation regime.<sup>36</sup> In contrast, broadband noise which covers all frequencies is a result of shockwaves generated by the occurrence of a violent inertial collapse of bubbles at large acoustic intensities and is indicative of inertial cavitation.<sup>28</sup> From the frequency spectrum (Figure 2a), only the fundamental frequency (1.1 MHz) was detected by the passive cavitation detection (PCD) at 0.16 MPa. This signal was likely due to weak reflection of the transmitted sound from the water–gel interface and not due to cavitation. Harmonics were detected from 0.32 MPa and were more pronounced at 0.64 MPa, which were indicative of stable cavitation typically observed from microbubbles.<sup>37</sup> When the pressure was increased to 0.96 MPa, the PCD detected both the broadband noise and the harmonics, which may be due to a mixture of stable cavitation and inertial cavitation occurring from the cavitation agent population. At 3.2 MPa, broadband emissions became dominant, showing that the bubbles violently collapsed and underwent intense inertial cavitation.<sup>38</sup> These violent collapses tend to emit shockwave pulses that are detected as broadband noise, hence the rise in baselines at the higher-pressure amplitudes.<sup>39</sup> As previously mentioned, stable

cavitation emitted higher harmonic emissions. Those harmonic emissions exponentially increased with an initial rapid that slowed as the pressure amplitude increased (Figure 2b). In contrast, broadband emissions increased following a power function. The stable and inertial cavitation thresholds (i.e., a 50% probability for an event to occur) were measured at 0.7 and 2.6 MPa, respectively. The probability for cavitation reached 100% at 1.1 MPa for stable cavitation and 3.2 MPa for inertial cavitation (Figure 2c). Therefore, the cavitation response of mcPLGA MPs may be adjusted to achieve the desired mechanical effect by changing the input acoustic pressure.

Samples of mcPLGA MPs were tested for contrast enhancement using a diagnostic ultrasound setup at 10 MHz with a mechanical index (MI) of 1.0. As can be seen in Figure 3, the mcPLGA MPs displayed the highest contrast enhancement with a CTR (contrast to tissue ratio) value of  $22.9 \pm 3.2$  dB, which is comparable to commercially available ultrasound contrast agents.<sup>30</sup> Nonporous hollow spherical PLGA microparticles (i.e., polymer microbubbles) with the same size (hsPLGA MPs, Figure S2) did not achieve substantial contrast enhancement ( $CTR = 7.2 \pm 2.9$  dB). One explanation for this discrepancy may be that, while the multicavity particles have surface stabilized gas bubbles that can nucleate at comparatively lower input pressures, the hollow spheres have a rigid polymer shell that needs higher pressures to either induce volumetric oscillations or rupture the shell to release the gas. Hence, at the pressure range tested, the multicavity variant provided a higher backscattered signal from these surface stabilized gas bubbles which are missing in the hollow variant. These results indicate that mcPLGA MPs were capable of nucleating cavitation to provide sufficient contrast enhancement for clinical imaging. Given that the mcPLGA MPs are of a clinically relevant size (1–5  $\mu\text{m}$ ) and that their response both

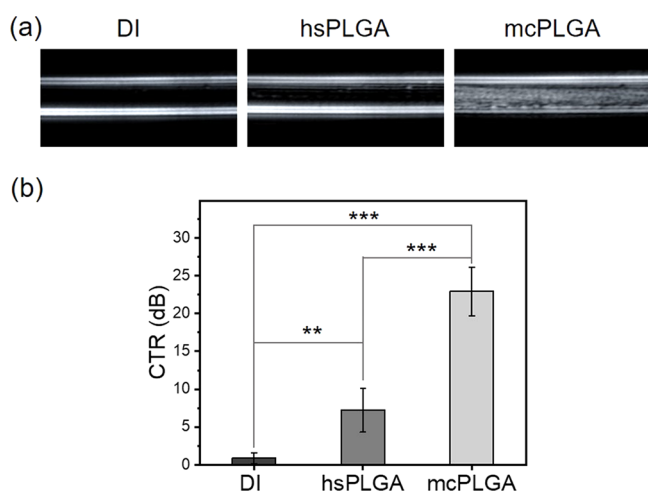


**Figure 3.** Contrast enhancement from mcPLGA MPs. (a) B mode ultrasound imaging with the diagnostic ultrasound scanner of DI water and 1 mg/mL suspensions of hollow sphere PLGA (hsPLGA) microparticles and mcPLGA MPs. (b) Corresponding CTR values of DI water, hsPLGA, and mcPLGA MPs (mean  $\pm$  SD,  $n = 3$ ). \*\* denotes a  $p < 0.01$  and \*\*\* denotes a  $p < 0.001$ .

deemed a murine model impractical to use. Larger animals (e.g., pig models) are challenging to use because building a robust atherosclerotic model remains difficult and costly. Instead, *in vitro* foam cell spheroid models were selected as the arterial model, because foam cells are responsible for the progression of atherosclerosis. Studying these foam cells will also elucidate the molecular processes that help determine the treatment efficacy of the therapeutic.<sup>41</sup> The foam cell spheroids were encapsulated in alginate beads ( $\sim 3$  mm) and then mounted next to the lumen of an agarose flow chamber prior to exposure to HIFU (Figure 4a). Before HIFU treatment, the foam cell spheroid structure was imaged with diagnostic ultrasound (10 MHz at 1.0 MI), which showed a predominantly hypoechoic region. Thereafter, the foam cell spheroid structure was treated with HIFU irradiation for 5 min (3.2 MPa, 5% duty cycle, 2 Hz RPF). Under these conditions, the mcPLGA MPs were site-specifically implanted into spheroid structures (Figure S3). These parameters are in line with *in vivo* ultrasound-mediated studies treating tumors<sup>28</sup> and opening blood-brain barrier,<sup>18</sup> and results have shown minimal damage to the surrounding tissues. After HIFU treatment, the lumen was flushed of mcPLGA MPs, and the spheroids were imaged using a conventional diagnostic ultrasound transducer (10 MHz at 1.0 MI). As can be seen from Figure 4b, the foam cell spheroids embeddings post-HIFU treatment were hyper-echoic under conventional B-mode imaging, with an image contrast  $15.2 \pm 1.6$  dB higher than pre-HIFU image.

The foam cell spheroids were also extracted from the spheroid embedment. This was achieved by dissolving the alginate beads using sodium citrate. After extraction, the foam cell spheroids were imaged by confocal microscopy to evaluate the penetration and distribution of RhB/DAPI coloaded

to HIFU and to diagnostic ultrasound is comparable to that of commercial contrast agents, these particles may be suitable as a theranostic agent.<sup>30,40</sup>

After confirming the cavitation threshold, we demonstrated targeted implantation of mcPLGA MPs into atherosclerotic models using acoustic cavitation. Considering that the arteries of a mouse are orders of magnitude smaller than that of a human and too small for the HIFU beam focal volume, we

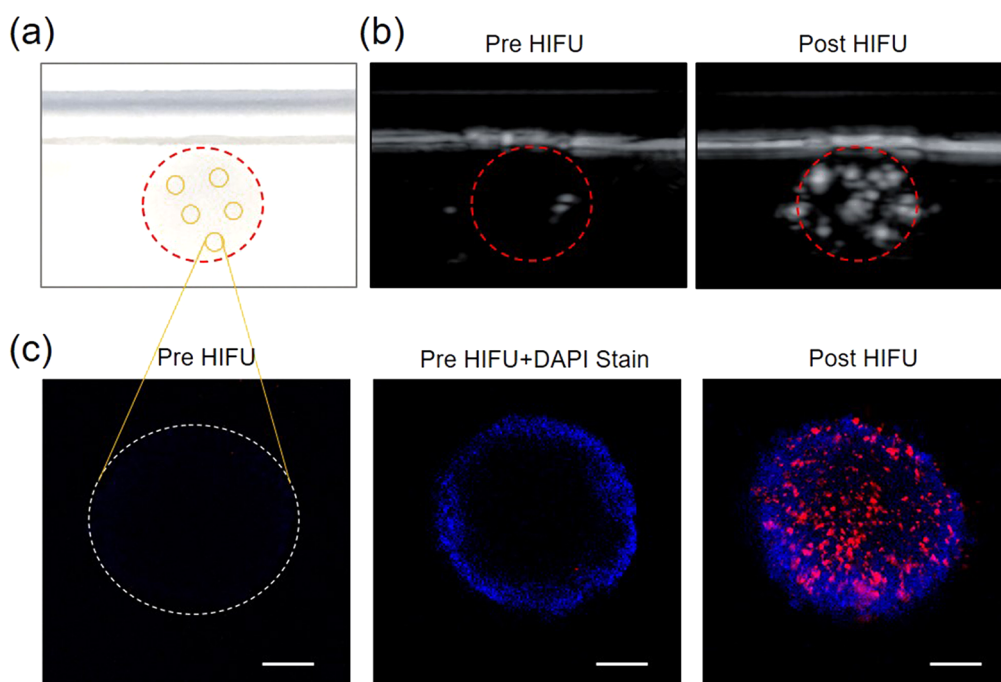


**Figure 4.** (a) Spheroids (indicated by the yellow cycles) embedded in alginate beads (indicated by the red dashed cycles). (b) B-mode ultrasound images of spheroids embedment before and after HIFU treatment. ROI is marked by red dashed cycles. (c) Confocal images of extracted foam cell spheroids. (Left) An image of a foam cell spheroid treated with 1 mg/mL mcPLGA MPs without HIFU exposure. (Middle) A similar foam cell spheroid treated with 1 mg/mL mcPLGA MPs without HIFU exposure but stained with DAPI to emphasize the diffusion limitation of cell spheroids. (Right) An image of a foam cell spheroid treated with 1 mg/mL mcPLGA MPs (loaded with DAPI and RhB) after HIFU exposure (right). The scale bars represent 100  $\mu$ m. mcPLGA MPs were indicated by red and DAPI fluorescence by blue.

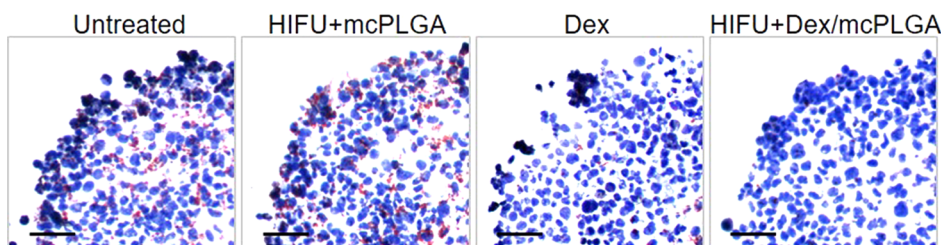


**Figure 5.** Oil Red O staining of foam cell spheroids under different treatment conditions. The scale bars represent 50  $\mu\text{m}$ .

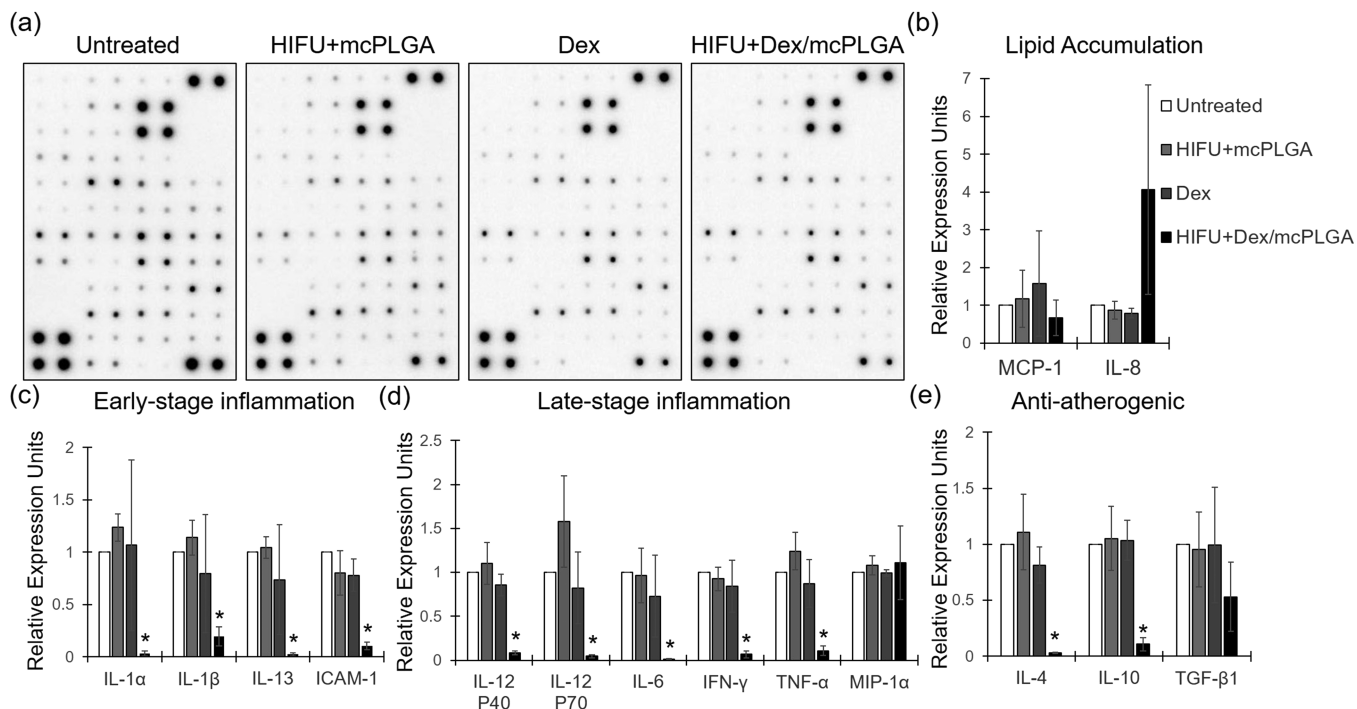


**Figure 6.** Estimation of cytokine release from foam cell spheroids. THP-1 derived foam cell spheroids exposed to HIFU+mcPLGA MPs, Dex alone, HIFU+Dex/mcPLGA MPs, or untreated. Supernatants were collected, and secreted cytokines were examined using a cytokine array. (a) Representative chemiluminescent images of cytokine array untreated or exposed to HIFU+mcPLGA MPs, Dex, or HIFU+Dex/mcPLGA MPs. Graphs showing quantification of the cytokine secretions categorized into three categories: (b) lipid accumulation, (c) early stage inflammation, (d) late-stage inflammation, and (e) anti-atherosclerotic cytokines. \* denotes a  $p < 0.05$  between the indicated groups and untreated controls.

374 mcPLGA MPs. Figure 4c showed fluorescent images of  
375 spheroids pre- and post-HIFU mediated implantation. Control  
376 spheroids without HIFU exposure showed a minimum  
377 presence of fluorescent particles. Then, the non-HIFU treated  
378 spheroids were stained with DAPI. DAPI staining exhibited  
379 strong fluorescence only in the outer edges of spheroids, due to  
380 limited permeability to diffuse deep into the core of the  
381 spheroid. In contrast, mcPLGA MPs penetrated and  
382 distributed throughout the entire spheroid in the presence of  
383 HIFU (Figures 4c and S4).

384 Here, we demonstrated the remote implantation of a  
385 biodegradable drug delivery vehicle into spheroids and  
386 enhance contrast after implantation. Conventional cavitation  
387 agents for drug delivery and imaging (i.e., microbubbles) are  
388 neither able to be implanted into tissue nor enhance contrast  
389 after implantation. Similarly, other solid cavitation nuclei  
390 decouple from the drug delivery vehicle, thereby limiting the  
391 penetration depth of the therapeutic and its dispersal into the  
392 tissue.<sup>28</sup> In our study, by coupling the therapeutic agent to  
393 biodegradable solid cavitation nuclei, we are able to  
394 demonstrate precise targeting of a drug with HIFU and  
395 verifying its delivery with contrast-enhanced ultrasound

imaging. As an ultrasound responsive vehicle actively driven 396  
by HIFU, these particles are able to be remotely implanted 397  
into the site of diseases, deliver therapeutics, and enhance 398  
contrast imaging of diseased tissue. Furthermore, the particles 399  
were not randomly distributed but were instead primarily 400  
accumulated within the beam focus of HIFU at the wall away 401  
from the HIFU transducer. This observation, the same with 402  
literature using different solid cavitation agents,<sup>28,29</sup> may be 403  
attributed to the cavitation nucleated from gas trapped on the 404  
particle cavities. These cavitation events, which only occur at 405  
the HIFU focus, likely created local microstreaming that in 406  
combination with acoustic radiation forces from the HIFU will 407  
transported particles away from the HIFU transducer and 408  
embedded them into tissue. Here, diagnostic ultrasound is 409  
used to verify the location of the particles post-HIFU 410  
treatment.<sup>42</sup> There are also other established methods, such 411  
as passive acoustic mapping, that may be used to monitor the 412  
treatment in real time.<sup>43</sup> 413

Given that mcPLGA MPs are capable of generating 414  
cavitation and propelling themselves into spheroids, we next 415  
demonstrated that site-specific delivery of Dex enhanced the 416  
lipid reduction in foam cell spheroids. Figure 5 shows 417



representative images of spheroids stained with Oil Red O and hematoxylin to show lipid (red) and nuclei (blue) under different treatment conditions after extraction and further culturing. Compared with untreated and HIFU+mcPLGA MPs treated samples, there was an expected reduction of oil droplets for spheroids treated with Dex alone. However, oil droplets near the core of the foam cell spheroid were still present due to diffusion limitations similar to our observations with DAPI staining. Interestingly, HIFU propelled Dex/mcPLGA MPs produced a more dramatic and uniform reduction of oil droplets compared to all the other treatment groups.

After qualitatively establishing the site-specific delivery of Dex/mcPLGA MPs into foam cell spheroids, we studied the effects of Dex/mcPLGA MPs on the inflammatory pathway under HIFU excitation. In order to achieve this, foam cell spheroids were untreated or exposed to HIFU+Dex/mcPLGA MPs. Additionally, the spheroids were also exposed to HIFU +mcPLGA MPs or Dex alone, to eliminate the possibility of either one of the conditions being responsible for the effect. Subsequently, the supernatants were collected and probed for secreted inflammatory cytokines (Figure 6a). After screening and analysis, the cytokines were grouped into 4 categories—(i) lipid accumulation, (ii) early stage inflammation, (iii) late-stage inflammation, and (iv) anti-atherogenic cytokines. It was noted that there was no significant difference in the secretion profile of cytokines MCP-1 and IL-8 which are responsible for lipid accumulation<sup>35,44</sup> by foam cells, upon exposure to the different treatments (Figure 6b). It is reported that oxidized low-density lipoprotein (oxLDL) induces early phase pro-inflammatory cytokines, triggering the “priming” of the inflammatory pathway by binding to Toll-like receptors (TLRs) or cluster of differentiation 36 (CD36) receptors on macrophage surfaces.<sup>45,46</sup> This step ensures activation of the NF $\kappa$ B pathway leading to transcriptional activation of components of the NLR family pyrin domain containing 3 (NLRP3)-inflammasome complex which regulates induction of caspase-1, and catalyzes the cleavage of pro-IL-1 $\beta$  and pro-IL-18, stimulating the secretion of the biologically active counterparts as well as IL-1 $\alpha$ .<sup>47,48</sup> Our results indicated that, upon exposure to HIFU +Dex/mcPLGA MPs, there was a significant reduction in secretion of IL-1 $\alpha$  and IL-1 $\beta$  (Figure 6c), which was not observed when the spheroids were exposed to either HIFU +mcPLGA MPs or Dex alone. Secretion of IL-1 $\alpha$  and IL-1 $\beta$  marks the initiation of the early inflammation phase along with cytokines including IL-10 and IL-13, which induce the recruitment of macrophages. Secretion of these cytokines was also reduced upon administration of HIFU+Dex/mcPLGA MPs (Figure 6c and e). Furthermore, a reduction in the levels of adhesion molecule ICAM-1 which recruit macrophages<sup>49</sup> to the endothelial wall (Figure 6c) was also observed. Again, there was no statistically significant effect of HIFU+PLGA MPs or Dex alone.

IL-1 $\beta$  and IL-18 activate late-stage pro-inflammatory cytokines. IL-1 $\beta$  induces secretion of IL-6, MIP-3 $\alpha$ , and TNF- $\alpha$ , while IL-18 induces IFN- $\gamma$ .<sup>45</sup> The current study corroborates this with the observed reduction of IL-12, IL-6, IFN- $\gamma$ , TNF- $\alpha$ , and MIP-1 $\alpha$  (Figure 6d) in HIFU+Dex/mcPLGA MPs treated conditions. The cytokines IL-6 and IL-12 work as a pair, whereby IL-6 promotes the release of tumor necrosis factor alpha (TNF- $\alpha$ ) and IL-1 $\alpha$  and induces formation of fatty streaks.<sup>50</sup> At the same time, IL-12 regulates differentiation of TH1 cells marking the completion of early-

stage atherosclerosis.<sup>50</sup> The most important pro-atherogenic cytokines are Interferon- $\gamma$  (IFN- $\gamma$ ) and TNF- $\alpha$ . IFN- $\gamma$  promotes uptake of oxLDL and foam cell formation, whereas TNF- $\alpha$  further promotes plaque formation and expression of monocyte chemoattractant protein-1 (MCP-1). MCP-1 and IL-8 are subsequently expressed in macrophages in response to cholesterol loading.<sup>45,50</sup>

Transforming growth factor- $\beta$  (TGF- $\beta$ ), IL-4, and IL-10 are anti-inflammatory cytokines.<sup>51</sup> These cytokines inhibit the Th1, Th2 cells and macrophages from proliferation, induction, and differentiation. However, our results indicate reduced secretion of IL-4 and IL-10 by foam cell spheroids exposed to HIFU+Dex/mcPLGA MPs, while there was no change in TGF- $\beta$  levels (Figure 6e). Both Dex and HIFU+mcPLGA MPs exposed spheroids did not show any significant difference. IL-10 is an anti-inflammatory cytokine which enhances oxLDL-induced foam cell formation, thus playing a protective role.<sup>52</sup> However, reduced levels of IL-10 may indicate reduced foam cells and thus reduced potential for plaque formation. Similarly, the role of IL-4 in atherosclerosis is not well understood, and there are contradictory reports.<sup>53–55</sup> Hence, further investigation of the role of HIFU+Dex/mcPLGA MPs on these anti-inflammatory cytokines and their overall impact on atherosclerosis will be beneficial, as our understanding of the function of these cytokines in terms of macrophage recruitment and foam cell development remains incomplete.

## 4. CONCLUSION

Here, we report on the HIFU-mediated implantation of a theranostic agent (mcPLGA MPs) for targeted drug delivery and contrast-enhanced ultrasound imaging. The degradable nature and unique surface structure of the designed mcPLGA MPs endowed the theranostic with distinctive advantages. After gas trapping, mcPLGA MPs nucleated both stable and inertial cavitation under exposure to HIFU at clinically relevant exposure conditions. We then showed that mcPLGA MPs were able to be remotely implanted into an *in vitro* 3D foam cell spheroid model with therapeutic ultrasound. Once implanted, mcPLGA MPs sustained the release of Dex, resulting in an enhanced therapeutic effect signified by a reduction in oxidized lipid levels and reduced secretion of pro-inflammatory cytokines in the foam cell spheroids. Under diagnostic ultrasound excitation, mcPLGA MPs showed a high contrast enhancement with a CTR value comparable to the commercially available ultrasound contrast agents after HIFU-induced implantation. Broadly, this novel and innovative method opens up a noninvasive route to monitor, improve, and verify treatment for inflamed arterial tissue as a result of atherosclerosis, angioplasty, and other peripheral vascular diseases.

## ■ ASSOCIATED CONTENT

### Supporting Information

The Supporting Information is available free of charge at <https://pubs.acs.org/doi/10.1021/acsami.1c01161>.

Spectral density curves of mcPLGA MPs; SEM and fluorescent images of hsPLGA MPs; fluorescence microscope image of spheroids embedment; fluorescence images of spheroids (PDF)

## AUTHOR INFORMATION

### Corresponding Authors

**Manojit Pramanik** – School of Chemical and Biomedical Engineering, Nanyang Technological University, 637459, Singapore; Email: [manojit@ntu.edu.sg](mailto:manojit@ntu.edu.sg)

**Kee Woei Ng** – School of Materials Science and Engineering, Nanyang Technological University, 639798, Singapore; Environmental Chemistry and Materials Centre, Nanyang Environment and Water Research Institution, 637141, Singapore; Center for Nanotechnology and Nanotoxicology, Harvard T.H. Chan School of Public Health, Harvard University, Boston, Massachusetts 02115, United States; [orcid.org/0000-0002-7276-3563](https://orcid.org/0000-0002-7276-3563); Email: [kwng@ntu.edu.sg](mailto:kwng@ntu.edu.sg), [kwng@hsph.harvard.edu](mailto:kwng@hsph.harvard.edu)

**James Kwan** – Department of Engineering Science, University of Oxford, Oxford OX3 7DQ, United Kingdom; [orcid.org/0000-0002-3795-6108](https://orcid.org/0000-0002-3795-6108); Email: [james.kwan@eng.ox.ac.uk](mailto:james.kwan@eng.ox.ac.uk)

### Authors

**Xiaoqian Su** – School of Chemical and Biomedical Engineering, Nanyang Technological University, 637459, Singapore; [orcid.org/0000-0002-8303-6660](https://orcid.org/0000-0002-8303-6660)

**Moumita Rakshit** – School of Materials Science and Engineering, Nanyang Technological University, 639798, Singapore

**Prativa Das** – School of Materials Science and Engineering, Nanyang Technological University, 639798, Singapore

**Ipshta Gupta** – School of Chemical and Biomedical Engineering, Nanyang Technological University, 637459, Singapore

**Dhiman Das** – School of Chemical and Biomedical Engineering, Nanyang Technological University, 637459, Singapore

Complete contact information is available at:

<https://pubs.acs.org/10.1021/acsami.1c01161>

### Author Contributions

\*X.S. and M.R. contributed equally. The manuscript was written through the contributions of all authors. All authors have given approval to the final version of the manuscript.

### Notes

The authors declare no competing financial interest.

## ACKNOWLEDGMENTS

This research is supported by the Ministry of Education in Singapore under the Tier 1 grant scheme (RG144/18, RG127/19), the Singapore Ministry of Health's National Medical Research Council under its NMRC/OFYIRG/0034/2017, and the NTU – Northwestern Institute for Nanomedicine (04INS000156C150).

## REFERENCES

- (1) Nakhband, A.; Eskandani, M.; Omid, Y.; Saeedi, N.; Ghaffari, S.; Barar, J.; Garjani, A. Combating Atherosclerosis with Targeted Nanomedicines: Recent Advances and Future Prospective. *BioImpacts* **2018**, *8*, 59.
- (2) Viles-Gonzalez, J. F.; Fuster, V.; Badimon, J. J. Atherothrombosis: A Widespread Disease with Unpredictable and Life-Threatening Consequences. *Eur. Heart J.* **2004**, *25*, 1197.
- (3) Lusis, A. J. Atherosclerosis. *Nature* **2000**, *407*, 233.

- (4) Maguire, E. M.; Pearce, S. W. A.; Xiao, Q. Foam Cell Formation: A New Target for Fighting Atherosclerosis and Cardiovascular Disease. *Vasc. Pharmacol.* **2019**, *112*, 54.
- (5) Bobryshev, Y. V.; Ivanova, E. A.; Chistiakov, D. A.; Nikiforov, N. G.; Orekhov, A. N. Macrophages and Their Role in Atherosclerosis: Pathophysiology and Transcriptome Analysis. *BioMed Res. Int.* **2016**, *2016*, 1.
- (6) Crowther, M. A. Pathogenesis of Atherosclerosis. *Hematology Am. Soc. Hematol. Educ. Program* **2005**, *2005*, 436.
- (7) Barnes, P. J. How Corticosteroids Control Inflammation: Quintiles Prize Lecture 2005. *Br. J. Pharmacol.* **2006**, *148*, 245.
- (8) Rhen, T.; Cidlowski, J. A. Antiinflammatory Action of Glucocorticoids — New Mechanisms for Old Drugs. *N. Engl. J. Med.* **2005**, *353*, 1711.
- (9) Tauchi, Y.; Takase, M.; Zushida, I.; Chono, S.; Sato, J.; Ito, K.; Morimoto, K. Preparation of a Complex of Dexamethasone Palmitate-Low Density Lipoprotein and Its Effect on Foam Cell Formation of Murine Peritoneal Macrophages. *J. Pharm. Sci.* **1999**, *88*, 709.
- (10) Tauchi, Y.; Zushida, I.; Chono, S.; Sato, J.; Ito, K.; Morimoto, K. Effect of Dexamethasone Palmitate-Low Density Lipoprotein Complex on Cholesterol Ester Accumulation in Aorta of Atherogenic Model Mice. *Biol. Pharm. Bull.* **2001**, *24*, 925.
- (11) Chono, S.; Morimoto, K. Uptake of Dexamethasone Incorporated into Liposomes by Macrophages and Foam Cells and Its Inhibitory Effect on Cellular Cholesterol Ester Accumulation. *J. Pharm. Pharmacol.* **2010**, *58* (9), 1219–1225.
- (12) Chono, S.; Tauchi, Y.; Deguchi, Y.; Morimoto, K. Efficient Drug Delivery to Atherosclerotic Lesions and the Antiatherosclerotic Effect by Dexamethasone Incorporated into Liposomes in Atherosclerotic Mice. *J. Drug Target.* **2005**, *13* (4), 267–276.
- (13) Sutton, J. T.; Haworth, K. J.; Pyne-Geithman, G.; Holland, C. K. Ultrasound-Mediated Drug Delivery for Cardiovascular Disease. *Expert Opin. Drug Delivery* **2013**, *10* (5), 573–592.
- (14) Gertz, Z. M.; Wilensky, R. L. Local Drug Delivery for Treatment of Coronary and Peripheral Artery Disease. *Cardiovasc. Ther.* **2011**, *29* (6), 54–66.
- (15) Panyam, J.; Labhasetwar, V. Biodegradable Nanoparticles for Drug and Gene Delivery to Cells and Tissue. *Adv. Drug Delivery Rev.* **2003**, *55* (3), 329–347.
- (16) Zhao, Y.; Zhu, Y.; Fu, J.; Wang, L. Effective Cancer Cell Killing by Hydrophobic Nanovoid-Enhanced Cavitation under Safe Low-Energy Ultrasound. *Chem. - Asian J.* **2014**, *9* (3), 790–796.
- (17) Myers, R.; Coviello, C.; Erbs, P.; Foloppe, J.; Rowe, C.; Kwan, J.; Crake, C.; Finn, S.; Jackson, E.; Balloul, J.; et al. Polymeric Cups for Cavitation-Mediated Delivery of Oncolytic Vaccinia Virus. *Mol. Ther.* **2016**, *24* (9), 1627–1633.
- (18) Abrahao, A.; Meng, Y.; Llinas, M.; Huang, Y.; Hamani, C.; Mainprize, T.; Aubert, I.; Heyn, C.; Black, S. E.; Hynynen, K.; et al. First-in-Human Trial of Blood–Brain Barrier Opening in Amyotrophic Lateral Sclerosis Using MR-Guided Focused Ultrasound. *Nat. Commun.* **2019**, *10* (1), 4373.
- (19) Lawrie, A.; Briskin, A. F.; Francis, S. E.; Cumberland, D. C.; Crossman, D. C.; Newman, C. M. Microbubble-Enhanced Ultrasound for Vascular Gene Delivery. *Gene Ther.* **2000**, *7*, 2023–2027.
- (20) Hernot, S.; Klivanov, A. L. Microbubbles in Ultrasound-Triggered Drug and Gene Delivery. *Adv. Drug Delivery Rev.* **2008**, *60* (10), 1153–1166.
- (21) Sirsi, S. R.; Borden, M. A. State-of-the-Art Materials for Ultrasound-Triggered Drug Delivery. *Adv. Drug Delivery Rev.* **2014**, *72*, 3–14.
- (22) Aryal, M.; Vykhodtseva, N.; Zhang, Y.-Z.; McDannold, N. Multiple Sessions of Liposomal Doxorubicin Delivery via Focused Ultrasound Mediated Blood–Brain Barrier Disruption: A Safety Study. *J. Controlled Release* **2015**, *204*, 60–69.
- (23) Fan, C. H.; Ting, C. Y.; Lin, H. J.; Wang, C. H.; Liu, H. L.; Yen, T. C.; Yeh, C. K. SPIO-Conjugated, Doxorubicin-Loaded Microbubbles for Concurrent MRI and Focused-Ultrasound Enhanced Brain-Tumor Drug Delivery. *Biomaterials* **2013**, *34* (14), 3706–3715.



- (24) Bazan-Peregrino, M.; Arvanitis, C. D.; Rifai, B.; Seymour, L. W.; Coussios, C. C. Ultrasound-Induced Cavitation Enhances the Delivery and Therapeutic Efficacy of an Oncolytic Virus in an in Vitro Model. *J. Controlled Release* **2012**, *157* (2), 235–242.
- (25) Stride, E. P.; Coussios, C. C. Cavitation and Contrast: The Use of Bubbles in Ultrasound Imaging and Therapy. *Proc. Inst. Mech. Eng., Part H* **2010**, *224* (2), 171–191.
- (26) Graham, S. M.; Carlisle, R.; Choi, J. J.; Stevenson, M.; Shah, A. R.; Myers, R. S.; Fisher, K.; Peregrino, M. B.; Seymour, L.; Coussios, C. C. Inertial Cavitation to Non-Invasively Trigger and Monitor Intratumoral Release of Drug from Intravenously Delivered Liposomes. *J. Controlled Release* **2014**, *178* (1), 101–107.
- (27) Zhao, Y.; Zhu, Y. Synergistic Cytotoxicity of Low-Energy Ultrasound and Innovative Mesoporous Silica-Based Sensitive Nanoagents. *J. Mater. Sci.* **2014**, *49* (10), 3665–3673.
- (28) Kwan, J. J.; Myers, R.; Coviello, C. M.; Graham, S. M.; Shah, A. R.; Stride, E.; Carlisle, R. C.; Coussios, C. C. Ultrasound-Propelled Nanocups for Drug Delivery. *Small* **2015**, *11* (39), 5305–5314.
- (29) Mannaris, C.; Teo, B. M.; Seth, A.; Bau, L.; Coussios, C.; Stride, E. Gas-Stabilizing Gold Nanocones for Acoustically Mediated Drug Delivery. *Adv. Healthcare Mater.* **2018**, *7* (12), 1800184.
- (30) Paefgen, V.; Doleschel, D.; Kiessling, F. Evolution of Contrast Agents for Ultrasound Imaging and Ultrasound-Mediated Drug Delivery. *Front. Pharmacol.* **2015**, *6*, 1 DOI: 10.3389/fphar.2015.00197.
- (31) Su, X.; Thomas, R. G.; Bharatula, L. D.; Kwan, J. J. Remote Targeted Implantation of Sound-Sensitive Biodegradable Multicavity Microparticles with Focused Ultrasound. *Sci. Rep.* **2019**, *9* (1), 1–13.
- (32) Su, X.; Gupta, I.; Jonnalagadda, U. S.; Kwan, J. J. Complementary Effects of Porosigen and Stabilizer on the Structure of Hollow Porous Poly(Lactic-Co-Glycolic Acid) Microparticles. *ACS Appl. Polym. Mater.* **2020**, *2* (8), 3696–3703.
- (33) Amatyia, S.; Park, E. J.; Park, J. H.; Kim, J. S.; Seol, E.; Lee, H.; Choi, H.; Shin, Y. H.; Na, D. H. Drug Release Testing Methods of Polymeric Particulate Drug Formulations. *J. Pharm. Invest.* **2013**, *43* (4), 259–266.
- (34) Gupta, I.; Su, X.; Jonnalagadda, U. S.; Das, D.; Pramanik, M.; Kwan, J. J. Investigating the Acoustic Response and Contrast Enhancement of Drug-Loadable PLGA Microparticles with Various Shapes and Morphologies. *Ultrasound Med. Biol.* **2021**, DOI: 10.1016/j.ultrasmedbio.2021.02.012.
- (35) Nguyen, L. T. H.; Muktabar, A.; Tang, J.; Wong, Y. S.; Thaxton, C. S.; Venkatraman, S. S.; Ng, K. W. The Potential of Fluocinolone Acetonide to Mitigate Inflammation and Lipid Accumulation in 2D and 3D Foam Cell Cultures. *BioMed Res. Int.* **2018**, *2018*, 1.
- (36) Tzanakis, I.; Lebon, G. S. B.; Eskin, D. G.; Pericleous, K. A. Characterizing the Cavitation Development and Acoustic Spectrum in Various Liquids. *Ultrason. Sonochem.* **2017**, *34*, 651.
- (37) Arvanitis, C. D.; Bazan-Peregrino, M.; Rifai, B.; Seymour, L. W.; Coussios, C. C. Cavitation-Enhanced Extravasation for Drug Delivery. *Ultrasound Med. Biol.* **2011**, *37*, 1838.
- (38) Kwan, J. J.; Graham, S.; Myers, R.; Carlisle, R.; Stride, E.; Coussios, C. C. Ultrasound-Induced Inertial Cavitation from Gas-Stabilizing Nanoparticles. *Phys. Rev. E* **2015**, *92* (2), No. 023019.
- (39) Cheng, M.; Li, F.; Han, T.; Yu, A. C. H.; Qin, P. Effects of Ultrasound Pulse Parameters on Cavitation Properties of Flowing Microbubbles under Physiologically Relevant Conditions. *Ultrason. Sonochem.* **2019**, *52*, 512–521.
- (40) Gupta, I.; Eisenbrey, J. R.; Machado, P.; Stanczak, M.; Wallace, K.; Forsberg, F. On Factors Affecting Subharmonic-Aided Pressure Estimation (SHAPE). *Ultrason. Imaging* **2019**, *41*, 35.
- (41) Neppiras, E. A. Subharmonic and Other Low-Frequency Emission from Bubbles in Sound-Irradiated Liquids. *J. Acoust. Soc. Am.* **1969**, *46* (3B), 587–601.
- (42) Abrahao, A.; Meng, Y.; Llinas, M.; Huang, Y.; Hamani, C.; Mainprize, T.; Aubert, I.; Heyn, C.; Black, S. E.; Hynynen, K.; et al. First-in-Human Trial of Blood–Brain Barrier Opening in Amyotrophic Lateral Sclerosis Using MR-Guided Focused Ultrasound. *Nat. Commun.* **2019**, DOI: 10.1038/s41467-019-12426-9.
- (43) Gray, M. D.; Elbes, D.; Paverd, C.; Lyka, E.; Coviello, C. M.; Cleveland, R. O.; Coussios, C. C. Dual-Array Passive Acoustic Mapping for Cavitation Imaging With Enhanced 2-D Resolution. *IEEE Trans. Ultrason. Ferroelectr. Freq. Control* **2021**, *68* (3), 647–663.
- (44) Wang, N.; Tabas, I.; Winchester, R.; Ravalli, S.; Rabbani, L. R. E.; Tall, A. Interleukin 8 Is Induced by Cholesterol Loading of Macrophages and Expressed by Macrophage Foam Cells in Human Atheroma. *J. Biol. Chem.* **1996**, *271*, 8837.
- (45) Miller, Y. I.; Chang, M. K.; Binder, C. J.; Shaw, P. X.; Witztum, J. L. Oxidized Low Density Lipoprotein and Innate Immune Receptors. *Curr. Opin. Lipidol.* **2003**, *14*, 437.
- (46) Endemann, G.; Stanton, L. W.; Madden, K. S.; Bryant, C. M.; White, R. T.; Protter, A. A. CD36 Is a Receptor for Oxidized Low Density Lipoprotein. *J. Biol. Chem.* **1993**, *268*, 11811.
- (47) Keller, M.; Rüegg, A.; Werner, S.; Beer, H. D. Active Caspase-1 Is a Regulator of Unconventional Protein Secretion. *Cell* **2008**, *132*, 818.
- (48) Kuida, K.; Lippke, J. A.; Ku, G.; Harding, M. W.; Livingston, D. J.; Su, M. S. S.; Flavell, R. A. Altered Cytokine Export and Apoptosis in Mice Deficient in Interleukin-1 $\beta$  Converting Enzyme. *Science* (Washington, DC, U. S.) **1995**, *267*, 2000.
- (49) Davies, M. J.; Gordon, J. L.; Gearing, A. J. H.; Pigott, R.; Woolf, N.; Katz, D.; Kyriakopoulos, A. The Expression of the Adhesion Molecules ICAM-1, VCAM-1, PECAM, and E-selectin in Human Atherosclerosis. *J. Pathol.* **1993**, *171*, 223.
- (50) Ramji, D. P.; Davies, T. S. Cytokines in Atherosclerosis: Key Players in All Stages of Disease and Promising Therapeutic Targets. *Cytokine Growth Factor Rev.* **2015**, *26* (6), 673–685.
- (51) Opal, S. M.; DePalo, V. A. Anti-Inflammatory Cytokines. *Chest* **2000**, *117* (4), 1162–1172.
- (52) Halvorsen, B.; Wæhre, T.; Scholz, H.; Clausen, O. P.; Von Der Thüsen, J. H.; Müller, F.; Heimli, H.; Tonstad, S.; Hall, C.; Frøland, S. S.; et al. Interleukin-10 Enhances the Oxidized LDL-Induced Foam Cell Formation of Macrophages by Antiapoptotic Mechanisms. *J. Lipid Res.* **2005**, *46*, 211.
- (53) Davenport, P.; Tipping, P. G. The Role of Interleukin-4 and Interleukin-12 in the Progression of Atherosclerosis in Apolipoprotein E-Deficient Mice. *Am. J. Pathol.* **2003**, *163*, 1117.
- (54) King, V. L.; Cassis, L. A.; Daugherty, A. Interleukin-4 Does Not Influence Development of Hypercholesterolemia or Angiotensin II-Induced Atherosclerotic Lesions in Mice. *Am. J. Pathol.* **2007**, *171*, 2040.
- (55) Wolfs, I. M. J.; Donners, M. M. P. C.; de Winther, M. P. J. Differentiation Factors and Cytokines in the Atherosclerotic Plaque Micro-Environment as a Trigger for Macrophage Polarisation. *Thromb. Haemostasis* **2011**, *106*, 763.